IOP Publishing Nanotechnology
Nanotechnology 29 (2018) 295202 (7pp) https://doi.org/10.1088/1361-6528/aac17d

In pursuit of barrierless transition metal dichalcogenides lateral heterojunctions

Yierpan Aierken[1], Cem Sevik[2], Oğuz Gülseren[3], François M Peeters[1] and Deniz Çakır[1,4]

[1] Department of Physics, University of Antwerp, Groenenborgerlaan 171, B-2020 Antwerpen, Belgium
[2] Department of Mechanical Engineering, Faculty of Engineering, Anadolu University, Eskisehir, TR 26555, Turkey
[3] Department of Physics, Bilkent University, Bilkent, Ankara 06800, Turkey
[4] Department of Physics and Astrophysics, University of North Dakota, Grand Forks, North Dakota 58202, United States of America

E-mail: deniz.cakir@und.edu

Received 13 February 2018, revised 23 April 2018
Accepted for publication 1 May 2018
Published 18 May 2018

Abstract

There is an increasing need to understand interfaces between two-dimensional materials to realize an energy efficient boundary with low contact resistance and small heat dissipation. In this respect, we investigated the impact of charge and substitutional atom doping on the electronic transport properties of the hybrid metallic-semiconducting lateral junctions, formed between metallic (1T and $1T_d$) and semiconducting (1H) phases of MoS_2 by means of first-principles and non-equilibrium Green function formalism based calculations. Our results clearly revealed the strong influence of the type of interface and crystallographic orientation of the metallic phase on the transport properties of these systems. The Schottky barrier height, which is the dominant mechanism for contact resistance, was found to be as large as 0.63 eV and 1.19 eV for holes and electrons, respectively. We found that armchair interfaces are more conductive as compared to zigzag termination due to the presence of the metallic Mo zigzag chains that are directed along the transport direction. In order to manipulate these barrier heights we investigated the influence of electron doping of the metallic part (i.e. $1T_d$-MoS_2). We observed that the Fermi level of the hybrid system moves towards the conduction band of semiconducting 1H-MoS_2 due to filling of 4*d*-orbital of metallic MoS_2, and thus the Schottky barrier for electrons decreases considerably. Besides electron doping, we also investigated the effect of substitutional doping of metallic MoS_2 by replacing Mo atoms with either Re or Ta. Due to its valency, Re (Ta) behaves as a donor (acceptor) and reduces the Schottky barrier for electrons (holes). Since Re and Ta based transition metal dichalcogenides crystallize in either the $1T_d$ or 1T phase, substitutional doping with these atom favors the stabilization of the $1T_d$ phase of MoS_2. Co-doping of hybrid structure results in an electronic structure, which facilities easy dissociation of excitons created in the 1H part.

Keywords: first-principles calculations, MoS_2, metal-semiconductor interface, Schottky barrier

(Some figures may appear in colour only in the online journal)

1. Introduction

Heterostructures are the essential components of a wide range of solid-state devices, such as transistors, solar cells, and sensors [1, 2]. They are fabricated by combining different type of materials, e.g. metal, semiconductor, and insulator. Therefore, the physical properties of the combined system are enhanced or become more controllable as compared to that of each material individually. These tailored properties are strongly related to the interface of two different materials where all interesting and new phenomenon occur. However, along with the emergence of nanostructured materials, dimensionality has become another major factor affecting the physical properties of materials and devices along with the

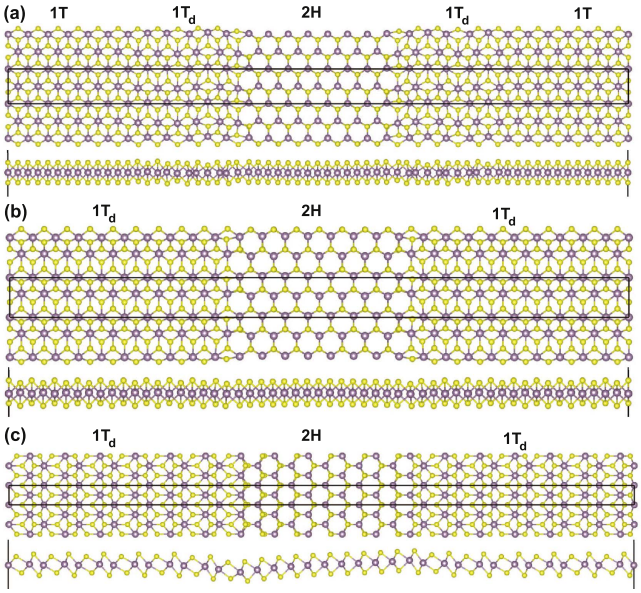

Figure 1. Device models where 1H phase of MoS_2 is sandwiched between metallic MoS_2 electrodes. In (a) the α-device, (b) the β-device, and (c) the γ-device. For the α and β devices, the interfaces between metallic and semiconducting MoS_2 have an armchair termination while a zigzag termination in the γ-device.

interface. Thus, solid-state device fabrication with heterostructures based on low dimensional nanomaterials has attracted significant attention and a new research area in material design has been initiated where researchers are expecting unprecedented results, phenomenon and physics [3–5]. Indeed, several advantages of two-dimensional (2D) phase engineering over the three dimensional counterpart has already been demonstrated [6].

In low dimensional heterostructure device architectures, there are usually two types of interfaces connecting different materials: top contact (vertical) and edge contact (lateral) [7]. In top contacts, an overlapping portion of two materials are glued together mainly via interlayer van der Waals (vdWs) interaction, while in edge contacts one dimensional edges of two materials are contacted with covalent bonds without overlapping. The vdWs interaction in top contact introduces a potential gap between the two layers which electrons have to tunnel through, and resulting in higher resistance due to the reduced carrier transmission probability. Naturally, this resistance is much lower in edge contacts owing to the formation of covalent bonds that provides a path for carriers to travel across the interfaces [8, 9]. Recently, Eda *et al* has discovered the coexistence of multi-phase MoS_2 that is a promising material for heterostructure device fabrication due to their natural metal-semiconductor-metal structure with clear edge contacts [10]. Considering the distinct electronic nature of these phases, physical properties of these heterostructures [11, 12] can be tuned by phase engineering and novel solid-state device architectures can be realized for several different future applications.

The same research group has synthesized 2D semiconducting heterostructure devices [13, 14] by using metal contacts. As a result of their experimental analysis, they have particularly pointed out the vital importance of the geometry and electronic nature consistency between the metal contact and the heterostructure on the device performance [10, 15]. Considering this fact, Kappera *et al* [11] have locally induced 1T metallic phase of MoS_2 in the 1H semiconducting phase of it, and they measured that the edge resistance was lower than that of metal contacts by more than a factor of two. Subsequently, 1T|1H lateral heterostructure has been drawn peculiar attention as a promising contact structure having a higher carrier injection rate. Different arrangements of the interfaces between 1T and 1H phases was investigated through theoretical calculations [16, 17] and the structure formed by the connection of armchair edges of 1T and 1H phases has been determined as an energetically more favorable configuration. However, in these calculations, the more stable metallic structure ($1T_d$), which arises with small distortion of 1T phase, was considered.

The use of metallic TMDCs as metal electrodes are expected to offer a breakthrough in the semiconductor industry as they have negligible heat dissipation and therefore are energy efficient. Among metallic TMDCs, metallic phases of MoS_2 (1T- and $1T_d$-MoS_2) have attracted a growing interest due to its smooth interface with the semiconductor phase of MoS_2 (1H-MoS_2). However, 1H phase is thermodynamically more stable than both 1T and $1T_d$ phases. Therefore, the stabilization of 1T and $1T_d$ over 1H phase becomes an essential requirement for the successful experimental realization of device configurable structures such as $1T/T_d$-MoS_2|1H-MoS_2. On the other hand, 1T-MoS_2 is the meta-stable and undergoes a Peierls transition to a low-energy state $1T_d$ (or distorted 1T) and thus, metal contacts with the $1T_d$ structure are more stable than the one with the 1T phase. However, the MoS_2 $1T_d$ phase retransforms to the 1H phase at room temperature. As far as the relative stability is considered, choosing $1T_d$ as metal contact further stabilized the junction. Therefore, understanding the effect of different physical mechanisms on the stability of multiple phases (H, T, T_d) of this material is of vital importance to develop a proper control on phase transitions. To this end, we mainly focus on the effect of doping (either charge or atom) on the stability, electronic and transport properties of $1T/T_d$-MoS_2|1H-MoS_2 interfaces.

The present paper aims to investigate the electronic transport properties of MoS_2 multi-phase lateral junctions when the more stable metallic phase of MoS_2 (i.e. $1T_d$) acts as the contact, which is compared with the 1T phase. Further to this, the paper mainly focuses on the effect of doping on the electrical transport properties. In the results section, we first construct three junction models and calculate their transmission without external bias . Then we calculate the electronic properties for different level of doping.

2. Computational details

The presented first-principles calculations are based on density function theory as implemented in the Vienna *ab initio* Simulation Package (VASP) [18–21]. A plane-wave basis set

based on the projected augmented wave method [22, 23] are used to describe the wave functions. The cutoff energy of the basis is set to 400 eV. Exchange-correlation interactions are treated with the generalized gradient approximation (GGA) within the Perdew–Burke–Ernzerhof (PBE) formulation [24, 25]. A 25 × 25 × 1 *k*-points mesh is used to sample the Brillouin-zone for monolayer structures of 1H, 1T and $1T_d$ MoS_2 and a 9 × 1 × 1 *k*-points grid is used for the structures shown in figure 1. A vacuum space of 15 Å is incorporated to avoid interaction between the periodic images. The energy convergence criterion for the self-consistent calculations is set to 10^{-5} eV, while the force convergence criterion for the ionic steps is set to 10^{-2} eV $Å^{-1}$.

Electronic transport across the $1T_d$/1T-MoS_2|1H-MoS_2 interfaces is calculated using the self-consistent non-equilibrium Green's functions technique as implemented in TranSIESTA [26] which is interfaced with the SIESTA code [27]. Double-zeta (plus polarization) numerical orbital basis sets are used for all atoms. We employed norm-conserving pseudo-potentials [28], the GGA/PBE functional, and an energy cutoff for the real-space mesh of 250 Ry. In order to get accurate transmission spectra, the 2D Brillouin-zone normal to the transport direction is sampled by meshes composed of 100 *k*-points in the periodic direction. While the SIESTA code uses a localized basis set and norm-conserving pseudo-potentials, the calculated lattice parameters for different phases of MoS_2 agree well with those obtained from the VASP code.

3. Results

We first calculate the structural properties of 1H, 1T and $1T_d$ phases of MoS_2. For the 1T and 1H hexagonal unit cells, the optimized in-plane lattice constant is obtained as 3.18 Å . On the other hand, the optimized lattice constants are $a = 3.18$ Å and $b = 5.72$ Å for the tetragonal $1T_d$ unit cell. These values are in good agreement with previous calculations [29]. It was previously discovered the coexistence of $1T_d$ phase with other two phases indicating their experimental stabilities, yet it is also possible to relax the $1T_d$ phase to to 1T phase using external source, such as electron beam irradiation [10]. In experiment, 1T and $1T_d$ are indistinguishable, because the S atoms are the same in two cases, only the Mo form cluster which STM image is limited to differentiate.

Next, we systematically investigate the electronic and transport properties of three different device architectures, called as α, β, and γ, denoted in figure 1. In all device models, the semiconducting 1H-MoS_2 phase is sandwiched between two $1T_d$ metal electrodes to create Schottky contacts at the interfaces. In the α structure, the metallic part consists of both 1T and $1T_d$-MoS_2 phases. The size of metallic and semiconducting parts are larger than 20 Å along the transport direction. The interface between the $1T_d$-MoS_2 and 1H-MoS_2 phases have either an armchair termination as in the case of the α and β structures, or a zigzag termination as in the case of the γ structure in order to investigate the influence of the contact type on the calculated properties. We predict that the

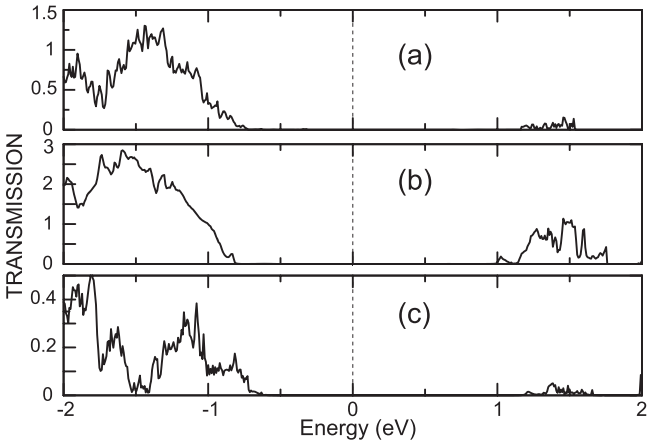

Figure 2. The zero bias transmission spectra for (a) the α-device, (b) the β device, and (c) the γ-device.

γ structure significantly deviates from planar geometry after structural relaxation, see figure 1. To check whether such distortion is due to a calculation artifact, we started from a complete planar geometry and allowed both atomic coordinates and cell parameters relax to their equilibrium values (or lowest energy configuration). We observed that planar structure is not stable and structural relaxation brought back the original distorted structure. Indeed, such buckling or deviation from planar structure mainly restricts to the left interface, in line with a recent work that proposed a new crystal structure model for MoS_2 [29]. Observed buckling helps to reduce repulsive interaction between S atoms at the left interface, thereby enhancing the stability of this interface.

The transmission spectra for all three device models at zero bias are depicted in figure 2. In these plots, the Schottky barrier for holes (electrons) is defined as the difference between Fermi level and valence band maximum (conduction band minimum) of the semiconductor 1H phase of MoS_2. The first clear observation is that there is a large barrier height at the pristine interfaces and there is no transmission within an energy range of 1.8 eV around the Fermi level, corresponding to the band gap of 1H-MoS_2. The Schottky barrier heights for the α, β and γ structures are predicted as 0.72, 0.80, and 0.63 eV for holes and 1.16, 0.99 and 1.19 eV for electrons, respectively. The estimated size of the scattering region along the transport direction is larger than 23 Å, which is much smaller than the mean free path of electron in MoS_2 [30] and therefore, the transport properties of these systems can be estimated with ballistic transport calculations. The β structure has the largest transmission over the calculated energy range. The Mo atoms form a zigzag chain perpendicular to the interface (or along the transport direction) in the β and also γ structures which enhances the electrical transport in these systems. However, the non-symmetric Mo zigzag chain lying parallel to the transport direction leads to scattering of electrons at the interface and gives rise to low transmission as compared to the α and β structures. Similar anisotropic electron transport has also been observed for ReS_2 where resistance is the lowest along the Re cluster direction [31]. Comparing the α and β devices, the coexistence of 1T and

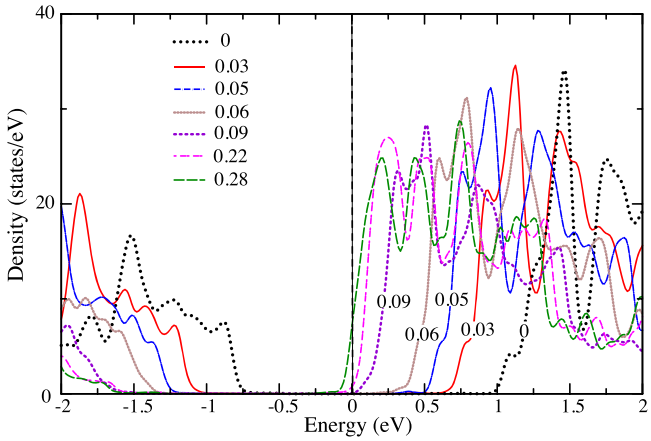

Figure 3. Projected density of states of the valence and conduction band of 1H-MoS_2 as a function of electron concentration for the β-device. Here, we only show the PDOS of the central part of 1H-MoS_2 where the effect of the interface is minimal. The Fermi level marks the zero energy. Electron concentrations (per formula unit of $1T_d$ phase) are given.

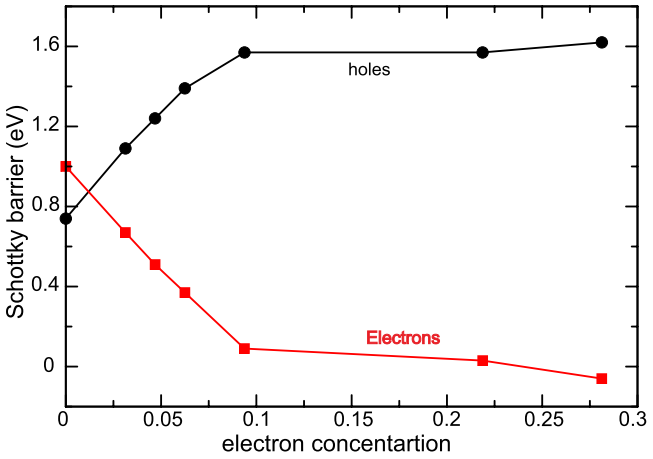

Figure 4. Variation of Schottky barrier for the β-device as a function of electron concentration (per formula unit of $1T_d$ part) for both electrons (red) and holes (black).

$1T_d$ regions in the former device contributes to lowering of the transmission due to additional scattering at the $1T/1T_d$ interface as compared to the latter device where we only have $1T_d$ phase in the electrode region.

We next turn to the calculations of the electronic properties as a function of doping. The central part of 1H-MoS_2 as the least affected from interface formation is considered to predict the band gap and the position of the band edges with respect to the Fermi level. Figure 3 shows the position of the Fermi level of the β structure with respect to the valence and conduction band of the central part of 1H-MoS_2 as a function of electron doping. The first observation is that the calculated band gap value of undoped MoS_2 (which is found to be 1.75 eV) clearly indicates that the size of the 1H part is large enough to achieve the monolayer limit and eliminates the electrode-electrode interaction. In fact, the band gap of the pristine 1H-MoS_2 monolayer calculated with the same functional is around 1.7 eV. In line with the transport calculations, the Fermi level appears within the band gap of the central region of 1H-MoS_2. The calculated Schottky barriers are 0.75 eV for holes and 0.99 eV for electrons in the β structure. In the following discussion, we mainly focus on the β structure due to its better transport properties as compared to the α and γ devices. Other device models also exhibit similar properties. Our results contradicts experimental findings in the sense that, in experiments, it was shown that 1T (or $1T_d$)|1H-MoS_2 interfaces exhibit a superior performance over the 3D metal-MoS_2 interfaces. However, we predict large Schottky barriers which give rise to a large contact resistance. In order to shed light on this contradiction, we calculate the electronic properties of the β structure as a function of electron doping. First of all, the electron doping stabilizes the $1T_d$ phase over the 1H-MoS_2 and prevents the structural phase transition to the semiconducting 1H-MoS_2 phase [32]. Also, the electron doping decreases the Schottky barrier height for electrons at the interface, leading to the formation of *n*-type Schottky barrier. This is attributed to the increase of the density of electrons in the *d*-orbital of the metallic $1T_d$ MoS_2 phase, see figure 3. Figure 4 shows the variation of the Schottky barrier as a function of the electron concentration. The Schottky barriers are calculated from figure 3. We find that the Schottky barrier already diminishes for electron concentration larger than 0.1 electron (per $1T_d$ MoS_2 formula unit). Here, 1 electron doping corresponds to a carrier density of $5.5 \times 10^{14}\,cm^{-2}$ using rectangular $1T_d$ unit cell. The Fermi level rises about 1 eV when 0.28 electron is placed on the $1T_d$ part. While the 0.3 electron doping per formula unit is a high doping limit, we can still achieve a 0.75 eV reduction of the Schottky barrier with a much smaller electron doping such as 0.06 electron per formula unit. Similarly, the Schottky barrier for holes is expected to be reduced by p-type doping (i.e. hole doping). The direct electron doping can be achieved by using electron beams in experiments or Li/Na adsorption on the metallic phase [32, 33] . Here, the considered alkali atoms donate their electron to the $1T_d$ phase and enhance the stability and electronic properties of the metallic part [32]. Charge doping lowers the transition barrier and induces a phase transition: 1H $\rightarrow$ 1T $\rightarrow$ $1T_d$. In addition, absorption of hydrogen atom on the 1T part of MoS_2 has been also shown to reduce the barrier at the interface of 1T-MoS_2|1H-MoS_2 [34, 35]. We can also realize either *n*-type or *p*-type doping of metallic phase of MoS_2 by using a suitable substrate. For instance, the calculated work function of 1H-MoS_2 is 5.2 eV. A low work function metal leads to electron doping in the 1H-MoS_2. As a result, we may have a structural phase transition from 1H to $1T_d$.

In lateral 2D heterostructures, the electronic band alignment is strongly dependent on the heterostructure width even in the absence of polar edges. In contrast to traditional 3D junctions, a highly non-localized charge transfer may be present in the lateral 2D junctions, which considerably increases the junction size [36–40]. Instead of having a narrow transition region between depleted region and neutral zone as in the case of 3D junctions, the transition region may even extend over entire devices in 2D junctions due to reduces electronic screening. In this respect, by enlarging the

1H-MoS_2 part and vacuum size, we performed test calculations to check the dependence of the Schottky barrier heights on the size of device region for the uncharged and charged system with 0.11 electron/f.u. In the new system, the size of the 1H-MoS_2 part and vacuum size are 57 Å and 20 Å, respectively. We found that the Schottky barrier changes by at most 0.05 eV.

Another possible strategy to enhance stability of metallic phases and electrical conduction at the metal-semiconductor MoS_2 interface is to dope metallic phase with transition metal atoms. Most of the well known TMDCs are either in the 1H or 1T phase when in their ground state. However, the single layer ReS_2 has neither H nor T as ground state, it stabilizes in $1T_d$ structure [41, 42]. Therefore, alloying MoS_2 with Re may stabilize the $1T_d$ structure of MoS_2 and leads to *n*-type doping of the crystal as similarly proposed by Raffone *et al* for Sn doped 1T phase [43]. Meanwhile, we have previously shown that doping of ReS_2 with Mo results in a *p*-type doping of ReS_2 monolayer [42]. Therefore, we investigated the effect of substitutional doping of Re at Mo sites of $1T_d$-MoS_2 on the transport properties. Here, we also considered the group V element Ta since the pristine TaS_2 monolayer crystallizes in the 1T phase and results in a *p*-type doped $1T_d$ MoS_2 structure. Indeed, in a recent work, it was shown that distorted phase of MoS_2 becomes energetically stable over 1H phase when Re concentration exceeds 50% [44]. In this work, we did not consider such large dopant concentrations because of two reasons. First of all, lattice mismatch between 1H-MoS_2 and doped 1T-MoS_2 phases can be kept minimal for small dopant concentrations. At large concentrations, the relaxation of cell parameters leads to artificial enlargement of lattice parameters of 1H-MoS_2. Secondly, Re-doped $1T_d$-MoS_2 becomes a semiconductor. To show the effect of doping, we only considered concentrations smaller than 20%. In addition, we only considered homogenous distribution of dopant atoms. In this work, we assumed that doping of 1T-MoS_2 with Re or Ta may avoid the structural transition to 1H phase due to, for instance, temperature effect. Figure 5 shows the PDOS for the central part of 1H-MoS_2 for Re and Ta-doped β structure. In the case of Re doping, the Fermi level approaches the conduction band of 1H-MoS_2, accompanying a significant decrease in *n*-type Schottky barrier height. On the other hand Ta doping reduces the *p*-type Schottky barrier height as expected. For a concentration of 14% (per electrode), the *n*-type Schottky barrier becomes 0.85 eV for Re and *p*-type Schottky barrier becomes 0.58 eV for Ta. We also checked the impact of the length of the 1H-MoS_2 part, which is 57 Å, on the electronic properties. Similar to previous case, we found that Re (Ta) doped system has lower Schottky barrier for holes (electrons) as compared to the pristine (i.e. undoped) system.

Since Re and Ta doping give rise to different electronic properties, we can design metal-semiconductor junctions with different type of Schottky barrier heights (i.e. *n*- and -*p* type) in the same device geometry. This allows us to design optical and photovoltaic applications. While a Re-doped junction effectively blocks holes, Ta-doped junction hampers the easy passage of electrons across the junction. In this device

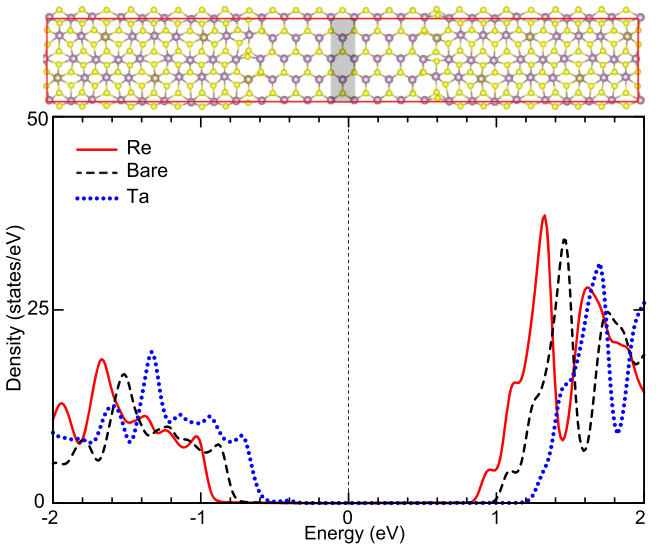

Figure 5. Projected density of states of the valence and conduction band of the central part of 1H-MoS_2 for Re and Ta-doped devices. In the top figure, gray region highlights the central part of 1H phase for which PDOS is calculated. For comparison, PDOS of bare device is also shown.

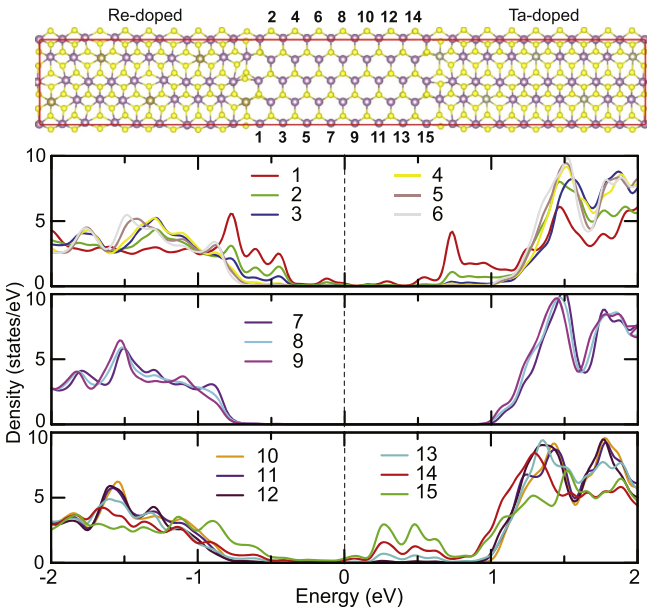

Figure 6. Projected density of states of 1H-MoS_2 at the different position on 1H-MoS_2. The Fermi level marks the zero energy.

geometry, we can separate photo-generated charge carriers for instance. Figure 6 shows the device model and projected density of states as a function of position in 1H-MoS_2. While the left electrode is doped with Re, the right electrode is alloyed with Ta. The central part of 1H-MoS_2 clearly has a PDOS similar to free standing 1H-MoS_2 monolayer with a band gap of 1.75 eV. However, we have different electronic properties in the right and left side of the central region. Due to Re (Ta) doping, the left (right) part has a *n* (*p*)-type Schottky barrier. The presence of $1T_d$-1H-MoS_2 interfaces develops mid-gap states that mainly come from the atoms in the boundary region. The electronic properties gradually

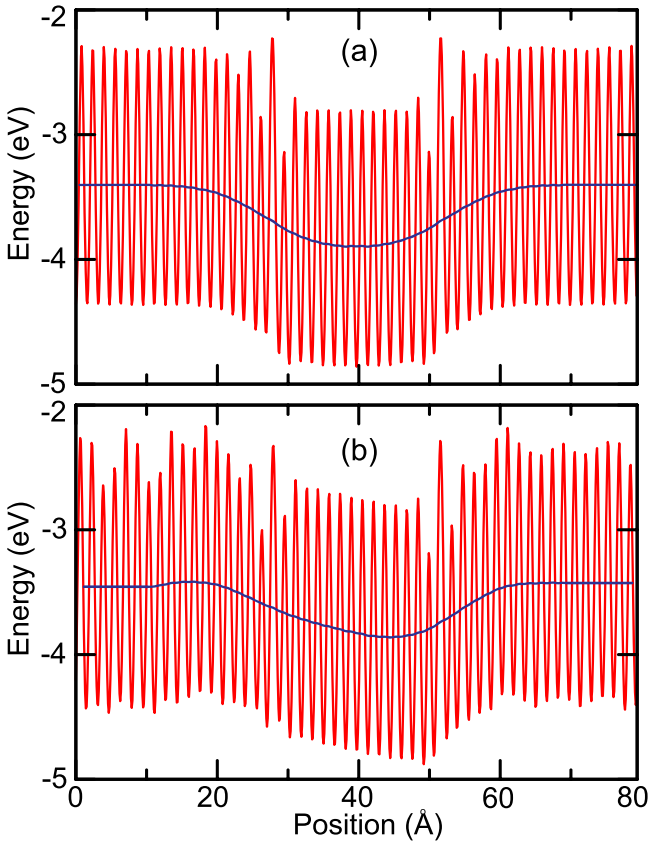

Figure 7. Self-consistent electrostatic potential profile along the interface of armchair (a) pristine and (b) doped $1T_d$-1H-$1T_d$ MoS_2 heterostructure. The right (left) $1T_d$ MoS_2 is doped with Re (Ta). Blue curve denotes the plane average potential along the heterostructure.

change from the metallic to the semiconductor when moving away from the interfaces. For the atoms far away from the interface region (i.e. central region of 1H-MoS_2), we observe a clear band gap which is close to that of pristine 1H-MoS_2. While the mid-gap states appear below the Fermi level at the left interface (Re-doped side), they are unoccupied and reside above the Fermi level at the right interface (Ta-doped side). About 3.2 Å from the interface, the mid-gap states start to disappear.

Figure 7 shows the electrostatic potential along the heterojunction. We consider both pristine and doped β-devices. For undoped heterojunction, the average potential is symmetric at the left and right interfaces. However, doped heterojunction has a different electrostatic potential, especially, within 1H-MoS_2. Due to its valence configuration, Re (Ta) acts as a donor (an acceptor). This is reflected in the average effective potential shown in figure 7(b). The average electrostatic potential (EP) does not have a sharp variation at the $1T_d$-1H interface, extending along the 2–3 atomic rows. This is due to fact that we form interfaces between two different crystal structures of MoS_2 (i.e $1T_d$ and 1H). EP converges to the same value at the left and right electrodes. If one considers a photovoltaic device using the β structure co-doped with Re and Ta, an electron–hole pair is generated after absorbing a photon in the 1H part. Re-doped interface has a higher potential as compared to Ta-doped interface, producing a driving force for dissociation of the electron–hole pair. The electron flows along the potential decline (i.e. towards Ta-doped electrode) and the hole in the opposite direction (i.e. towards Re-doped electrode). In this way, a photocurrent can be generated by the photovoltaic effect. Thus, by proper control of doping and interface roughness, we can control the quantum efficiency of electron–hole dissociation [45].

4. Conclusion

In this work, we explored the impact of doping on the electronic and charge transport properties across the $1T_d$-1H-MoS_2 interfaces by considering various device models. Doping and alloying (with charge, atom or molecule) appear as an effective method to tailor and improve the physical-chemical properties and stabilities of not only $1T/1T_d$ phases of MoS_2 but also other 2D materials. The interface structure between $1T_d$ and 1H phases is one of the decisive factors in the determination of the electrical transport across the heterojunction. We found that the Schottky barrier height of electrons for pristine heterojunctions can even disappear as a result of electron doping. While charge doping only reduces the Schottky barrier for electrons, co-doping is able to tune the barriers for hole and electrons at the same time.

Acknowledgments

This work was supported by the bilateral project between the The Scientific and Technological Research Council of Turkey (TUBITAK) and FWO-Flanders, Flemish Science Foundation (FWO-Vl) and the Methusalem foundation of the Flemish government. Computational resources were provided by TUBITAK ULAKBIM, High Performance and Grid Computing Center (TRGrid e-Infrastructure), and HPC infrastructure of the University of Antwerp (CalcUA) a division of the Flemish Supercomputer Center (VSC), which is funded by the Hercules foundation. We acknowledge the support from TUBITAK (Grant No. 115F024).

ORCID iDs

Deniz Çakır https://orcid.org/0000-0003-3315-5204

References

[1] Singh J 1993 *Physics of Semiconductors and Their Heterostructures* (*Electrical Engineering Series*) (New York: McGraw-Hill)
[2] Agostini G and Lamberti C 2011 *Characterization of Semiconductor Heterostructures and Nanostructures* (Amsterdam: Elsevier)

[3] Gan L-Y, Zhang Q, Cheng Y and Schwingenschlögl U 2013 *Phys. Rev.* B **88** 235310
[4] Wu N, Yang Z, Zhou W, Zou H, Xiong X, Chen Y and Ouyang F 2015 *J. Appl. Phys.* **118** 084306
[5] Bartolomeo A D 2016 *Phys. Rep.* **606** 1
[6] Duerloo K-A N and Reed E J 2016 *ACS Nano* **10** 289
[7] Allain A, Kang J, Banerjee K and Kis A 2015 *Nat. Mater.* **14** 1195
[8] Matsuda Y, Deng W-Q and Goddard W A 2010 *J. Phys. Chem.* C **114** 17845
[9] Kang J, Liu W, Sarkar D, Jena D and Banerjee K 2014 *Phys. Rev.* X **4** 031005
[10] Eda G, Fujita T, Yamaguchi H, Voiry D, Chen M and Chhowalla M 2012 *ACS Nano* **6** 7311
[11] Kappera R, Voiry D, Yalcin S E, Branch B, Gupta G, Mohite A D and Chhowalla M 2014 *Nat. Mater.* **13** 1128
[12] Fan X, Xu P, Zhou D, Sun Y, Li Y C, Nguyen M A T, Terrones M and Mallouk T E 2015 *Nano Lett.* **15** 5956
[13] Huang C, Wu S, Sanchez A M, Peters J J P, Beanland R, Ross J S, Rivera P, Yao W, Cobden D H and Xu X 2014 *Nat. Mater.* **13** 1096
[14] Zhang X-Q, Lin C-H, Tseng Y-W, Huang K-H and Lee Y-H 2015 *Nano Lett.* **15** 410
[15] Bai Z, Markussen T and Thygesen K S 2013 arXiv:1311.2393
[16] Hu Z, Zhang S, Zhang Y-N, Wang D, Zeng H and Liu L-M 2015 *Phys. Chem. Chem. Phys.* **17** 1099
[17] Sivaraman G, de Souza F A L, Amorim R G, Scopel W L, Fyta M and Scheicher R H 2016 *J. Phys. Chem.* C **120** 23389
[18] Kresse G and Hafner J 1993 *Phys. Rev.* B **47** 558
[19] Kresse G and Hafner J 1994 *Phys. Rev.* B **49** 14251
[20] Kresse G and Furthmüller J 1996 *Comput. Mater. Sci.* **6** 15
[21] Kresse G and Furthmüller J 1996 *Phys. Rev.* B **54** 11169
[22] Blöchl P E 1994 *Phys. Rev.* B **50** 17953
[23] Kresse G and Joubert D 1999 *Phys. Rev.* B **59** 1758
[24] Perdew J P, Burke K and Ernzerhof M 1996 *Phys. Rev. Lett.* **77** 3865
[25] Perdew J P, Burke K and Ernzerhof M 1997 *Phys. Rev. Lett.* **78** 1396
[26] Brandbyge M, Mozos J-L, Ordejón P, Taylor J and Stokbro K 2002 *Phys. Rev.* B **65** 165401
[27] Soler J M, Artacho E, Gale J D, Garcia A, Junquera J, Ordejón P and Sanchez-Portal D 2002 *J. Phys.: Condens. Matter* **14** 2745
[28] Troullier N and Martins J L 1991 *Phys. Rev.* B **43** 1993
[29] Ma F, Gao G, Jiao Y, Gu Y, Bilic A, Zhang H, Chen Z and Du A 2016 *Nanoscale* **8** 4969
[30] Radisavljevic B, Radenovic A, Brivio J, Giacometti V and Kis A 2011 *Nat Nanotechnol.* **6** 147
[31] Lin Y-C, Komsa H-P, Yeh C-H, Bjrkman T, Liang Z-Y, Ho C-H, Huang Y-S, Chiu P-W, Krasheninnikov A V and Suenaga K 2015 *ACS Nano* **9** 11249
[32] Kan M, Wang J Y, Li X W, Zhang S H, Li Y W, Kawazoe Y, Sun Q and Jena P 2014 *J. Phys. Chem.* C **118** 1515
[33] Katagiri Y *et al* 2016 *Nano Lett.* **16** 3788
[34] Nourbakhsh A *et al* 2016 *Nano Lett.* **16** 7798
[35] Tang Q and Jiang D-E 2015 *Chem. Mater.* **27** 3743
[36] Leenaerts O, Vercauteren S and Partoens B 2017 *Appl. Phys. Lett.* **110** 181602
[37] Zhang J, Xie W, Zhao J and Zhang S 2017 *2D Mater.* **4** 015038
[38] Yu H, Kutana A and Yakobson B I 2016 *Nano Lett.* **16** 5032
[39] Cheng K, Guo Y, Han N, Su Y, Zhang J and Zhao J 2017 *J. Mater. Chem.* C **5** 3788
[40] Leenaerts O, Vercauteren S, Schoeters B and Partoens B 2016 *2D Mater.* **3** 025012
[41] Tongay S *et al* 2014 *Nat. Commun.* **5** 3252
[42] Cakir D, Sahin H and Peeters F M 2014 *Phys. Chem. Chem. Phys.* **16** 16771
[43] Raffone F, Ataca C, Grossman J C and Cicero G 2016 *J. Phys. Chem. Lett.* **7** 2304
[44] Tan T L, Ng M-F and Eda G 2016 *J. Phys. Chem.* C **120** 2501
[45] Cao Z, Harb M, Lardhi S and Cavallo L *J. Phys Chem. Lett.* **8** 1664 pMID: 28332394